**Central European Journal of Energetic Materials**
ISSN 1733-7178; e-ISSN 2353-1843


*Cent. Eur. J. Energ. Mater.* 2021, *18*(2): 245-270; DOI 10.22211/cejem/139396
Article is available in PDF-format, in colour, at:
https://ipo.lukasiewicz.gov.pl/wydawnictwa/cejem-woluminy/vol-18-nr-2/


***Research paper***

# Detonation Characteristics of Gaseous Isopropyl Nitrate at High Concentrations

Linghui Zeng, Huimin Liang, Qi Zhang*

*State Key Laboratory of Explosion Science and Technology, Beijing Institute of Technology, 100081 Beijing, China*
* *E-mail:* qzhang@bit.edu.cn

**Abstract:** Isopropyl nitrate (IPN) is a component of propellant fuel. High concentrations of IPN can still produce detonation. To date, very limited literature is available regarding high concentrations of IPN detonations. The detonation pressure is related to the equivalence ratio and density of IPN/air mixtures. These two factors have opposing effects on the detonation of an IPN/air mixture. The detonation characteristics of gaseous IPN/air mixtures at high concentrations (300-4000 g/m$^3$) have been studied numerically. The results showed that when the IPN concentration is 300-600 g/m$^3$, density played a dominant role on detonation. The maximum detonation pressure, 2.81 MPa, and the maximum detonation velocity, 1890 m/s, occurred at a concentration of 600 g/m$^3$ (equivalence ratio $\Phi = 2.15$). When the IPN concentration was increased from 300 to 600 g/m$^3$, the peak overpressure and velocity increased by 19.6% and 6.2%, respectively. When the IPN concentration is higher than 600 g/m$^3$, the equivalence ratio is extremely large and the detonation properties were seriously degraded. An analysis of the detonation products illustrated the burn-off rate of high concentrations of IPN and the influence of the detonation product $CH_3CHO$. At a concentration of 600 g/m$^3$, the IPN/air mixture can achieve optimal detonation properties and fuel economy.

**Keywords:** isopropyl nitrate, detonation properties, detonation products, fuel-rich, numerical simulation

**Nomenclature:**

$a$ Absorption coefficient
$E$ Total energy [J]
$f_d$ Diffuse fraction
$\vec{F}$ External body force [N]
$g_i$ Gravitational vector in the $i$ direction [N]
$G_b$ Turbulence kinetic energy due to buoyancy [J]
$G_k$ Turbulence kinetic energy due to the mean velocity gradients [J]
$h$ Sensible enthalpy [J]
$I$ Radiation intensity [W/m$^2$]
$\vec{J}_j$ Diffusion flux
$k$ Thermal conductivity [W/m·K]
$M_{w,i}$ Molecular weight of species $i$ [g]
$n$ Refractive index
$p$ *S*tatic pressure [Pa]
$Pr_t$ Turbulent Prandtl number (0.85)
$r$ Radial coordinate
$\vec{r}$ Position vector
$R_i$ Net rate of production
$\hat{R}_{i,r}$ Arrhenius molar rate of creation of species $i$ in reaction $r$
$s$ Path length [m]
$\vec{s}$ Direction vector
$\vec{s}'$ Scattering direction vector
$S_h$ Heat of chemical reaction [J]
$S_i$ Rate of creation
$S_m$ Mass source
$T$ Local temperature [K]
$v_n$ Particle velocity normal to the wall [m/s]
$v_r$ Radial velocity [m/s]
$v_x$ Axial velocity [m/s]
$v_y$ Swirl velocity [m/s]
$x$ Axial coordinate
$Y_i$ Local mass fraction
$Y_M$ Fluctuating dilatation [1/K]
$\rho$ Fluid density [kg/m$^3$]
$\mu$ Molecular viscosity [mPa·s]
$\varepsilon$ Rate of dissipation
$\varepsilon_w$ Wall emissivity [W/m$^2$·K$^4$]
$\sigma$ Stefan-Boltzmann constant ($5.669 \cdot 10^{-8}$ W/m$^2$·K$^4$)

$\sigma_S$ Scattering coefficient
$\Phi$ Phase function
$\Omega'$ Solid angle

## 1 Introduction

Isopropyl nitrate (IPN, $C_3H_7NO_3$) is a component of propellant fuel. It is widely used in petroleum, aerospace and other fields. At present, many applications, such as a propellant fuel [1] or a fuel additive [2] for detonation propulsion systems, have been developed. As a high-performance fuel, IPN is known for its non-toxicity, non-corrosiveness, low cost, high explosion sensitivity and wide explosion concentration limit (2-100%) [3]. These physical and chemical properties make IPN important as an ignition [4] or detonation promoter [5]. However, when the vapour of the fuel is mixed with air and reaches a certain concentration during transportation or emission, it is very likely to burn or even explode [6]. The low security of IPN hinders its industrial use. Based on the isopropyl nitrate explosion accident in a Danish factory, Hedlund *et al.* [7] summarized similar accidents that have occurred in the last 15 years. This study showed that a high concentration fuel/air mixture is likely to be formed during production and transportation, confirming the strong detonation properties of high concentrations of IPN. Therefore, a study of the detonation characteristics of high concentrations of IPN has an important guiding significance for evaluating fuel properties, optimizing fuel efficiency and improving production safety.

Many experiments and numerical simulations have been carried out on the detonation of IPN/air mixtures. Ambekar *et al.* [8] experimentally studied the combustion and detonation characteristics of monopropellant IPN. The effect of ambient pressure and the burning rates of IPN was elucidated. Liu *et al.* [9] studied and analyzed the characteristics and stages of the deflagration-to-detonation transition (DDT) in IPN/air mixtures. The minimum DDT concentration of the mixture was determined to be 450 g/m$^3$. Sheffield *et al.* [10] studied the detonation process of IPN and predicted the Hugoniot state of IPN. The IPN detonation wave produced super detonation at the initial impact stage and finally developed into stable detonation. Nassim *et al.* [11] used Kissinger's method, Equation of State (EOS) method and Maxwell's approximation method to calculate the detonation parameters of mixtures with different concentrations of IPN. The lower explosive limit [12] and minimum ignition energy [13, 14] of IPN have also been discussed. Most of the above researches used the minimum free energy and the Chapman-

Jouguet (CJ) detonation theory in their calculations. The IPN discussed in these studies was at a relatively low concentration (around the stoichiometric concentration). However, IPN can also detonate at high concentrations and there are few studies of this.

For a high concentration of IPN, the detonation parameters depends on the equivalence ratio and the density of the IPN/air mixture. With an increase in density, the detonation properties will be increased correspondingly [15]. However, when the concentration is higher than the stoichiometric concentration (285 g/m$^3$), the matching relationship between combustible elements and oxygen elements deteriorates. The detonation properties cannot increase continuously due to oxygen deficiency [16]. Fuel density and equivalence ratio have different effects on detonation. Determining the critical values of these two factors is helpful for fuel optimization. In the present study, the detonation process of IPN/air mixtures is numerically simulated. The detonation characteristics of gaseous IPN at high concentrations were determined by CFD numerical calculation.

## 2 Governing Equations

In this study, the continuous phase model was used to solve the Navier-Stokes equation of 2D compressible reaction flow. The discrete ordinates (DO) model was adopted. The governing equations were chosen with their axisymmetric form.

(1) Mass conservation equation [17]:

$$\frac{\partial \rho}{\partial t} + \frac{\partial}{\partial x}(\rho v_x) + \frac{\partial}{\partial r}(\rho v_r) + \frac{\rho v_r}{r} = S_m \tag{1}$$

(2) Momentum conservation equations [18]:

The axial and radial momentum conservation equations are given by:

$$\frac{\partial}{\partial t}(\rho v_x) + \frac{1}{r}\frac{\partial}{\partial x}(r\rho v_x v_x) + \frac{1}{r}\frac{\partial}{\partial r}(r\rho v_r v_x) = -\frac{\partial p}{\partial x} + \frac{1}{r}\frac{\partial}{\partial x}\left[r\mu\left(2\frac{\partial v_x}{\partial x} - \frac{2}{3}(\nabla \cdot \vec{v})\right)\right] + \frac{1}{r}\frac{\partial}{\partial r}\left[r\mu\left(\frac{\partial v_x}{\partial r} + \frac{\partial v_r}{\partial x}\right)\right] + F_x \tag{2}$$

$$\frac{\partial}{\partial t}(\rho v_r) + \frac{1}{r}\frac{\partial}{\partial x}(r\rho v_x v_r) + \frac{1}{r}\frac{\partial}{\partial r}(r\rho v_r v_r) = -\frac{\partial p}{\partial r} + \frac{1}{r}\frac{\partial}{\partial x}\left[r\mu\left(\frac{\partial v_r}{\partial x} + \frac{\partial v_x}{\partial r}\right)\right] + \frac{1}{r}\frac{\partial}{\partial r}\left[r\mu\left(2\frac{\partial v_r}{\partial r} - \frac{2}{3}(\nabla\cdot\vec{v})\right)\right] - 2\mu\frac{v_r}{r^2} + \frac{2}{3}\frac{\mu}{r}(\nabla\cdot\vec{v}) + \rho\frac{v_z^2}{r} + F_r \quad (3)$$

(3) Energy conservation equation:

$$\frac{\partial}{\partial t}(\rho E) + \nabla\cdot\left(\vec{v}(\rho E + p)\right) = \nabla\cdot\left[k_{eff}\nabla T - \sum_j h_j\overrightarrow{J_J} + (\bar{\bar{\tau}}\cdot\vec{v})\right] + S_h \quad (4)$$

(4) Chemical species transport equation [19]:

$$\frac{\partial}{\partial t}(\rho Y_i) + \nabla\cdot(\rho\vec{v}Y_i) = -\nabla\cdot\overrightarrow{J_i} + R_i + S_i \quad (5)$$

$$R_i = M_{w,i}\sum_{r=1}^{N_R}\hat{R}_{i,r} \quad (6)$$

(5) Standard *k*-*ε* model [20]:

The turbulence kinetic energy ($k$) and its rate of dissipation ($\varepsilon$) are given by:

$$\frac{\partial}{\partial t}(\rho k) + \frac{\partial}{\partial x_i}(\rho k u_i) = \frac{\partial}{\partial x_j}\left[\left(\mu + \frac{\mu_t}{\sigma_k}\right)\frac{\partial k}{\partial x_j}\right] + G_k + G_b - \rho\varepsilon - Y_M \quad (7)$$

$$\frac{\partial}{\partial t}(\rho\varepsilon) + \frac{\partial}{\partial x_i}(\rho\varepsilon u_i) = \frac{\partial}{\partial x_j}\left[\left(\mu + \frac{\mu_t}{\sigma_\varepsilon}\right)\frac{\partial\varepsilon}{\partial x_j}\right] + C_{1\varepsilon}\frac{\varepsilon}{k}(G_k + C_{3\varepsilon}G_b) - C_{2\varepsilon}\rho\frac{\varepsilon^2}{k} \quad (8)$$

The model constants had the following values: $C_{1\varepsilon}$ = 1.44, $C_{2\varepsilon}$ = 1.92, $\sigma_k$ = 1.0, and $\sigma_\varepsilon$ = 1.3.

(6) The DO radiation model [21]:

The DO radiation model can solve the radiative transfer equation for heat transfer and reflection on the wall. The equation is written as:

$$\nabla\cdot[I(\vec{r},\vec{s})\vec{s}] + (a+\sigma_s)I(\vec{r},\vec{s}) = an^2\frac{\sigma T^4}{\pi} + \frac{\sigma_s}{4\pi}\int_0^{4\pi} I\left(\vec{r},\vec{s}'\right)\Phi\left(\vec{s},\vec{s}'\right)d\Omega' \quad (9)$$

If  is the amount of radiative energy incident on the opaque wall, then the following general quantities may be computed for opaque walls:

- Emission from the wall surface = $n^2\varepsilon_w\sigma T_w^4$
- Diffusely reflected energy = $f_d(1-\varepsilon_w)q_{in}$
- Specularly reflected energy = $(1-f_d)(1-\varepsilon_w)q_{in}$
- Absorption at the wall surface = $\varepsilon_w q_{in}$

(7) Boundary condition [22]:

The boundary condition solves the momentum loss and reflection on the wall.

$$e_n = \frac{v_{2,n}}{v_{1,n}} \tag{10}$$

(8) Chemical reaction:

It was assumed that the air in the detonation tube is composed of 21% oxygen and 79% nitrogen by volume. In the oxygen-rich state, the combustion of IPN can be simplified as an overall one step reaction [23]. The chemical reaction of a gaseous IPN/air mixture with a stoichiometric volume fraction is as follows:

$$C_3H_7NO_3 + 3.25(O_2 + 3.76N_2) \rightarrow 3.5H_2O + 3CO_2 + 12.72N_2 \tag{11}$$

The fuel mass concentration and volume fraction of IPN under the conditions of chemical equivalence $\Phi = 1$ are shown as follows:

$$c_{mass,IPN} = \frac{M_{IPN}}{V_{total}} = \frac{105}{1\times22.4+3.25(1+3.76)\times22.4} \times 10^3 \approx 285 \text{ g/m}^3 \tag{12}$$

$$c_{vol,IPN} = \frac{V_{IPN}}{V_{total}} = \frac{1}{1+3.25(1+3.76)} \approx 6.07 \text{ vol/\%} \tag{13}$$

For IPN in an oxygen-rich reaction, the specific parameters are listed in Table 1.

**Table 1.** Simulation parameters of IPN in an oxygen-rich reaction

| Parameter | Units | Value |
|---|---|---|
| Molecular weight | [kg/kmol] | 105 |
| Activation energy [24] | [J/kmol] | $1.24 \cdot 10^8$ |
| Pre-exponential factor [25] | [kmol/(m$^3$·s)] | $5 \cdot 10^{10}$ |
| Standard state enthalpy [26] | [J/kmol] | $-1.8408 \cdot 10^8$ |
| Standard state entropy [27] | [J/kmol·K] | $3.74 \cdot 10^5$ |
| Specific heat ratio [28] | – | piecewise linear of temperature |

However, for high concentrations of IPN, the oxygen in the combustion reaction is insufficient. Beeley *et al.* [29] studied the IPN reaction under oxygen-poor conditions. They detected the intermediates and found that under any experimental conditions, cleavage of the $(CH_3)_2CHO–NO_2$ bonds was the only way to react in the first step. Zeng *et al.* [30] showed that the cleavage of $(CH_3)_2CHO–NO_2$ bonds is the main reaction of IPN

thermal decomposition. The isopropoxy group is then split to form $CH_3$ and $CH_3CHO$. Therefore, the decomposition of IPN produces a large number of gaseous intermediates, which has a large impact on the detonation characteristics. The following intermediate reaction processes also need to be considered in the numerical calculations:

$$(CH_3)_2CHONO_2 \rightarrow (CH_3)_2CHO + NO_2 \quad (14)$$

$$(CH_3)_2CHO \rightarrow CH_3 + CH_3CHO \quad (15)$$

For IPN in an oxygen-poor reaction, the specific parameters are listed in Table 2.

**Table 2.** Simulation parameters of IPN in an oxygen-poor reaction

| Parameter | Units | Value |
|---|---|---|
| Activation energy [31] | [J/kmol] | $1.77 \cdot 10^8$ |
| Heat of formation [32] | [J/kmol] | $-1.91 \cdot 10^6$ |
| Decomposition rates [33] | [kmol/(m$^3$·s)] | $2.309 \cdot 10^9$ |
| Specific heat ratio [34, 35] | – | piecewise linear of temperature |

## 3 Model

It was assumed that gaseous IPN is uniformly mixed with the tube air before ignition. The diameter and length of the detonation tube were 0.06 and 1.00 m, respectively. The tube was closed at both ends. According to the axisymmetric property of the model, half of the flow field was taken as the computing domain. The simplified two-dimensional axisymmetric model and nine monitoring points are shown in Figure 1. The ignition region is a semicircle with a radius of 1.5 cm at the left end of the tube, with an ignition pressure 10 MPa and an ignition temperature 3000 K. The remaining region was at standard atmospheric pressure and temperature. A boundary of a rigid and adiabatic wall was adopted.

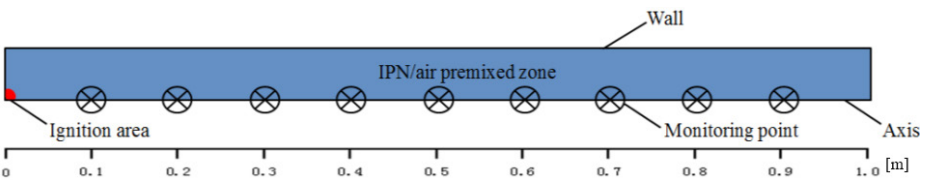


**Figure 1.** Computational model of the detonation tube

In this study, the detonation characteristics of IPN were calculated for a range of concentrations, from 300 to 4000 g/m$^3$. To facilitate comparison of the numerical results, Table 3 lists the mass concentrations and fractions of the fuel/air mixtures at different equivalence ratios.

**Table 3.** Mass concentrations and mass fractions of the IPN/air mixtures

| Mass concentration [g/m$^3$] | Mass fraction [%] | Volume fraction [%] | Equivalence ratio $\Phi$ | Oxygen ratio [%] |
|---|---|---|---|---|
| 300 | 20.00 | 6.43 | 1.08 | 26.84 |
| 600 | 33.33 | 12.06 | 2.15 | 31.17 |
| 1000 | 45.45 | 18.61 | 3.59 | 32.52 |
| 2000 | 62.50 | 31.40 | 7.18 | 36.19 |
| 4000 | 76.92 | 47.79 | 14.35 | 39.47 |

## 3.1 Verification of grid independence

In order to determine the required resolution for simulations of IPN/air mixtures, three different numerical grid sizes were adopted to test the grid independence. The grid sizes were 0.1, 0.05, and 0.01 mm, respectively. In this verification, the IPN concentration in the tube was 300 g/m$^3$. Monitoring points were set at 0.3, 0.6 and 0.9 m from the left end, respectively. Figure 2 plots the overpressure time-history curves for the three grids.

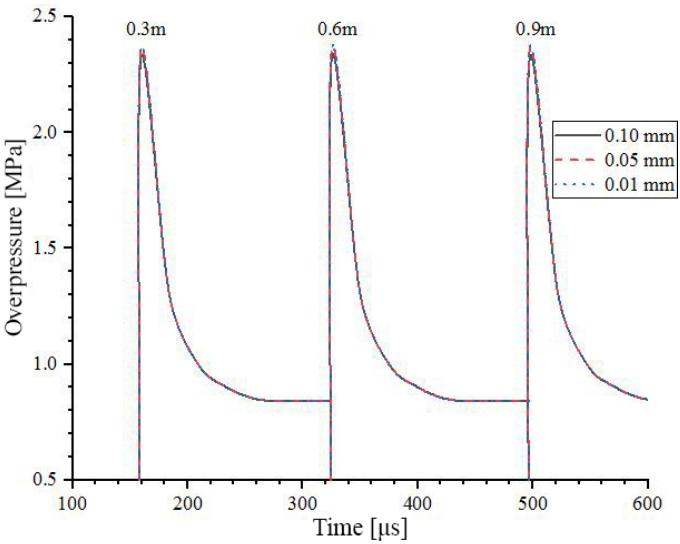


**Figure 2.** Overpressure time-history curves for the three grids

The simulated overpressures for the three grid sizes tend essentially to a constant value of the CJ pressure and the experimental results of IPN detonation [9]. Table 4 lists the comparison of the peak overpressures. The results show that when the grid size is reduced to 0.05 mm, the peak overpressure tends to be stable. To balance calculation accuracy and efficiency, the 0.05 mm grid, consisting of 12,000,000 quadrilateral cells, was used in the calculations.

**Table 4.** Comparison of peak overpressures for the three grids

| Grid size [mm] | Grid quantity | Peak overpressure [MPa] | Discrepancy from the 0.01 mm grid [%] |
|---|---|---|---|
| 0.1 | 3,000,000 | 2.336 | 0.89 |
| 0.05 | 12,000,000 | 2.351 | 0.25 |
| 0.01 | 300,000,000 | 2.357 | – |

## 3.2 Verification of the numerical method

For verification of the numerical method, the IPN/air mixture previously studied by Liu *et al.* [9] was simulated under the same experimental conditions. The experimental tube was 199 mm in diameter and 28 m long. The specific experimental parameter settings are listed in Table 5.

**Table 5.** Experimental parameters [9]

| Parameter | Unit | Value |
|---|---|---|
| Ignition energy | [J] | 40 |
| Ignition radius | [mm] | 1.5 |
| Initial temperature | [K] | 294 |
| Initial pressure | [MPa] | 0.14 |
| IPN concentration | [g/m$^3$] | 400/473/590 |

The detonation process of IPN/air mixtures at three different concentrations was simulated. Figure 3 shows the detonation pressure curves obtained by experiment and simulation. The peak overpressures obtained by simulation were 2.31 MPa (400 g/m$^3$), 4.45 MPa (473 g/m$^3$) and 4.01 MPa (590 g/m$^3$). The experimental data were slightly lower. The peak overpressures were 2.10, 4.30 and 3.90 MPa, respectively.

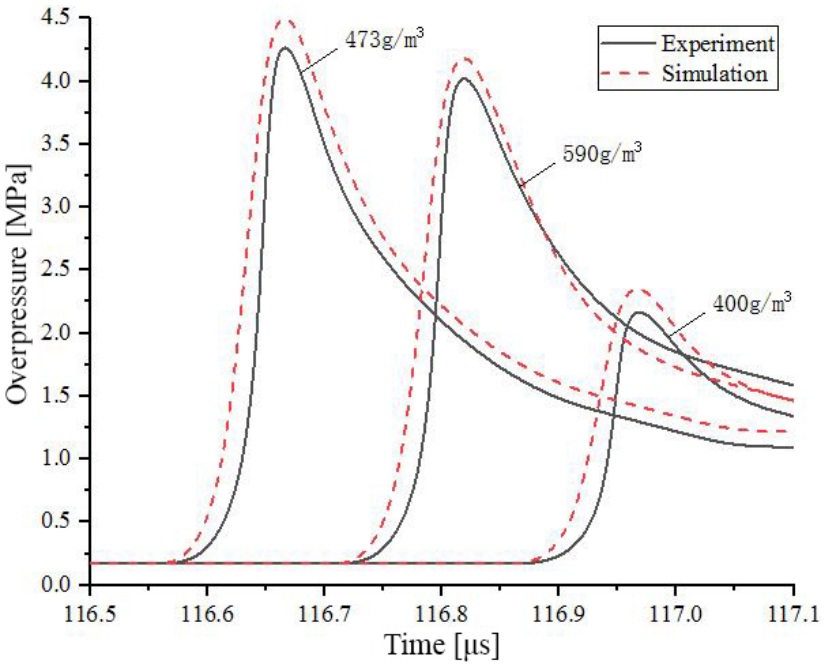


**Figure 3.** Comparison of simulated overpressure with experimental data

The maximum errors of the simulated overpressure curves were 9.1% (400 g/m$^3$), 3.4% (473 g/m$^3$) and 2.7% (590 g/m$^3$) compared with the experimental data. The curvilinear trend matched well. In the experiment, IPN fuel was not as evenly distributed in the container as in the simulated case, and there was a certain fuel loss. Therefore, it is reasonable that the peak values of the curves obtained by simulation were slightly higher than the experimental data. The errors are within the acceptable range, so the numerical model and solution method can be considered to be accurate.

## 4 Results and Discussion

### 4.1 Detonation pressure

Figure 4 shows the overpressure propagation process of the IPN/air mixture at a concentration of 300 g/m$^3$ exploding along the tube axis. The dark coloured area on the right of the wave front represents the unburned zone, and the light coloured area on the left represents the reaction product zone. After ignition, the explosion overpressure propagates stably until it reaches the right end.

A high pressure region behind the wave exists for a short time. The red coloured area represents the high pressure region, and its peak overpressure is within 2.4 MPa. There is a certain loss of energy on the wall. The detonation overpressure attenuates along the r-axis. The surface of the detonation wave is curved. The detonation velocity is highest on the central axis. As time increases, this phenomenon becomes more obvious. Other concentrations of the mixture exhibited similar propagation processes. As a strong ignition source ignites the premixed gases, leading shock waves are generated in the early stage of detonation, which will eventually develop into a stable detonation. The phenomenon is quite consistent with the earlier literature [36].

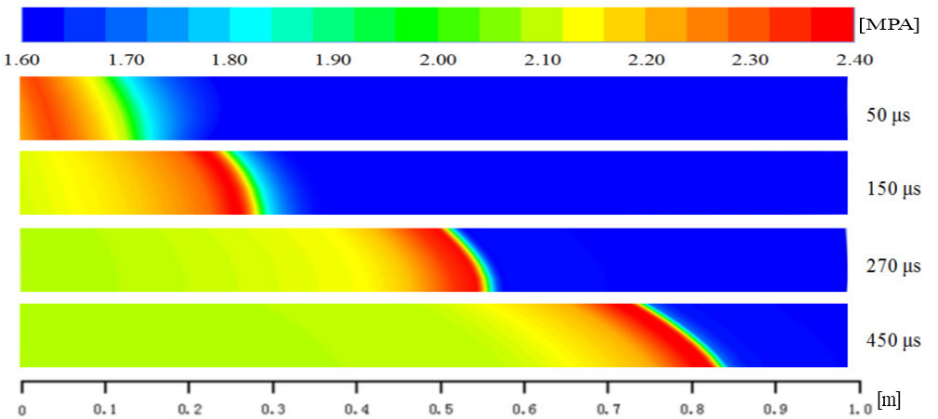


**Figure 4.** Overpressure propagation process of the IPN/air mixture (300 g/m$^3$)

Figure 5 shows the detonation pressure of mixtures with different concentrations of IPN/air. The maximum peak overpressure reached 2.81 MPa at a concentration of 600 g/m$^3$. The peak overpressure obtained at 1000 g/m$^3$ was slightly lower, at 2.47 MPa. The peak overpressures obtained at 300 and 1000 g/m$^3$ were very close. The peak overpressure of 4000 g/m$^3$ was the lowest, only 1.72 MPa. It can be found that when the concentration is increased from 600 to 4000 g/m$^3$, the concentration is increased by 567%, while the pressure is decreased by 1.09 MPa, about 39%. Moreover, the peak arrival time of the 4000 g/m$^3$ mixture was the latest, followed by the 2000 g/m$^3$ mixture. The peak arrival times of the other concentrations were close.

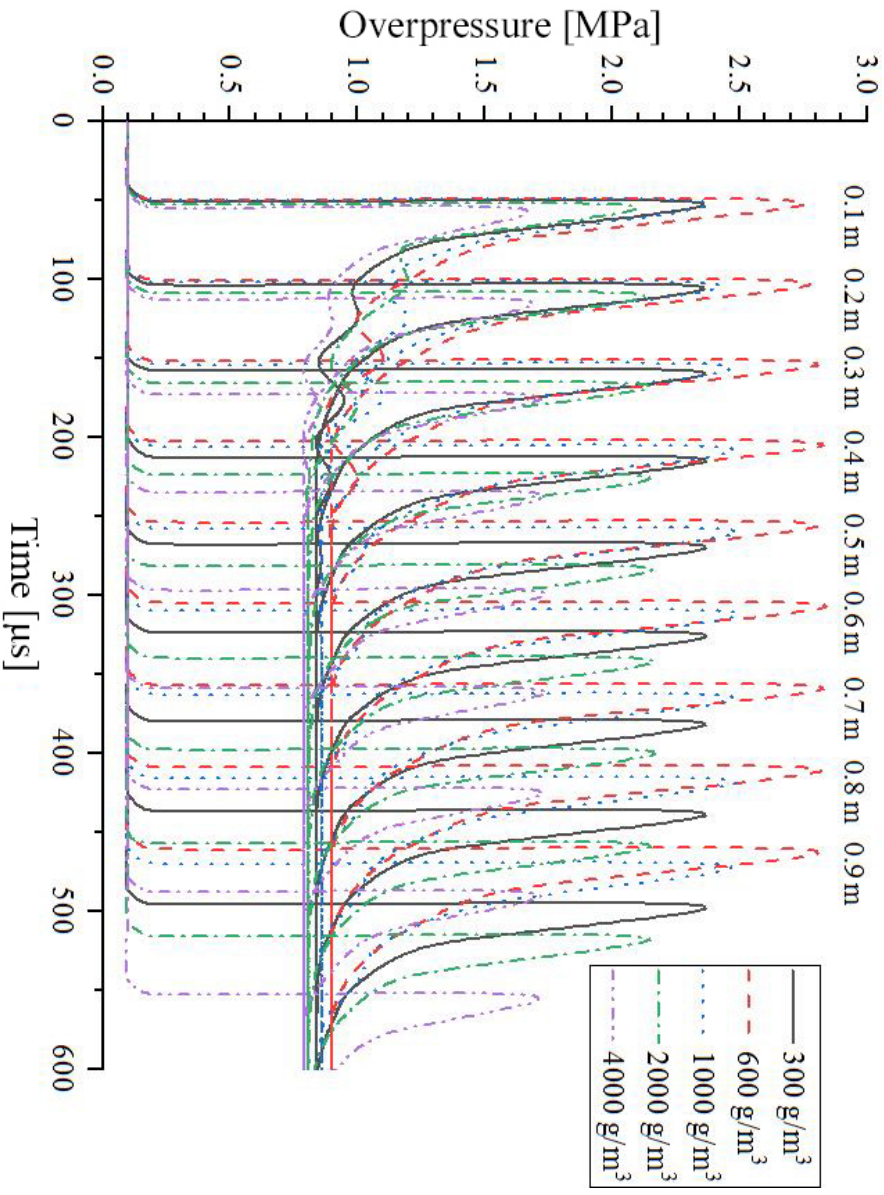


**Figure 5.** Detonation pressures of IPN/air mixtures at different concentrations

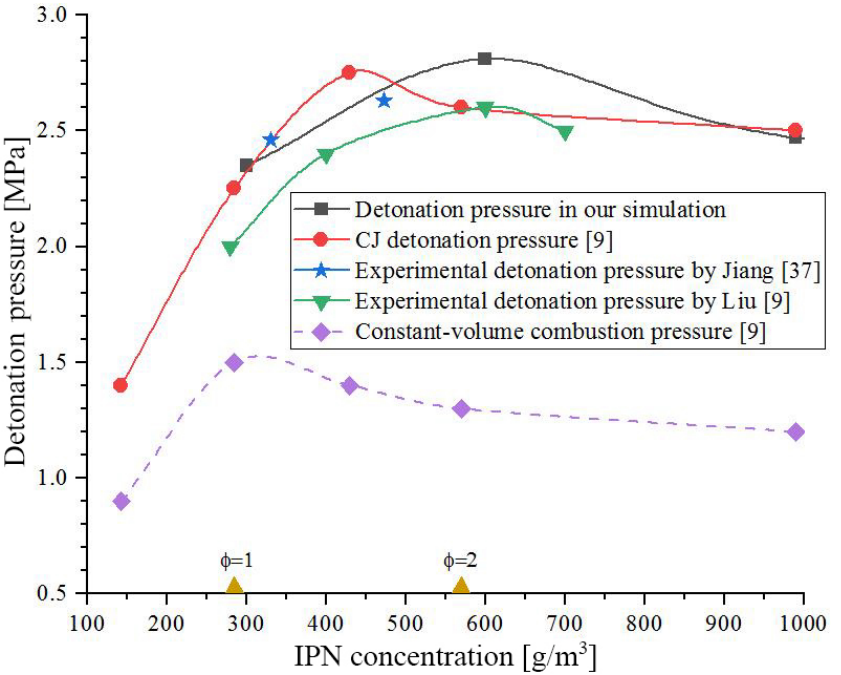


**Figure 6.** Detonation pressure from experiments and simulation

Figure 6 shows the detonation peak overpressures at different concentrations. The results show that the maximum detonation overpressure of IPN in the tube does not occur at the stoichiometric concentration (285 g/m$^3$), but at a higher concentration (600 g/m$^3$, equivalence ratio $\Phi = 2.15$). When the concentration is between 300 and 600 g/m$^3$, the increase in fuel density provides a large amount of reactant for the thermal decomposition reaction. A large amount of IPN produces high-temperature and high-pressure gas (mainly $CH_3CHO$). The detonation overpressure continues to rise with concentration. When the concentration is higher than 600 g/m$^3$, the fuel-rich state dominates and the detonation overpressure begins to drop. The reaction of IPN is inhibited at very high concentrations.

The results can be compared with the experimental detonation pressure [9, 37] and the CJ detonation pressure. The simulated pressures are about 0.2 MPa higher than the experimental pressures reported by Liu *et al.* [9]. This is because the fuel and oxygen in the simulation are evenly mixed in the tube. The chemical reactions in the simulation are more complete than those in the experiment, and the pressures obtained are higher. It is worth noting that both the simulated and experimental pressure peaks occur around $\Phi = 2$. Compared with the CJ detonation pressure, these trends in the pressure peaks are consistent. At the same time, the simulated

pressure is more than twice the combustion pressure, which proves the strength and reliability of the simulated detonation process. The simulated pressures are in good agreement with the experimental pressures.

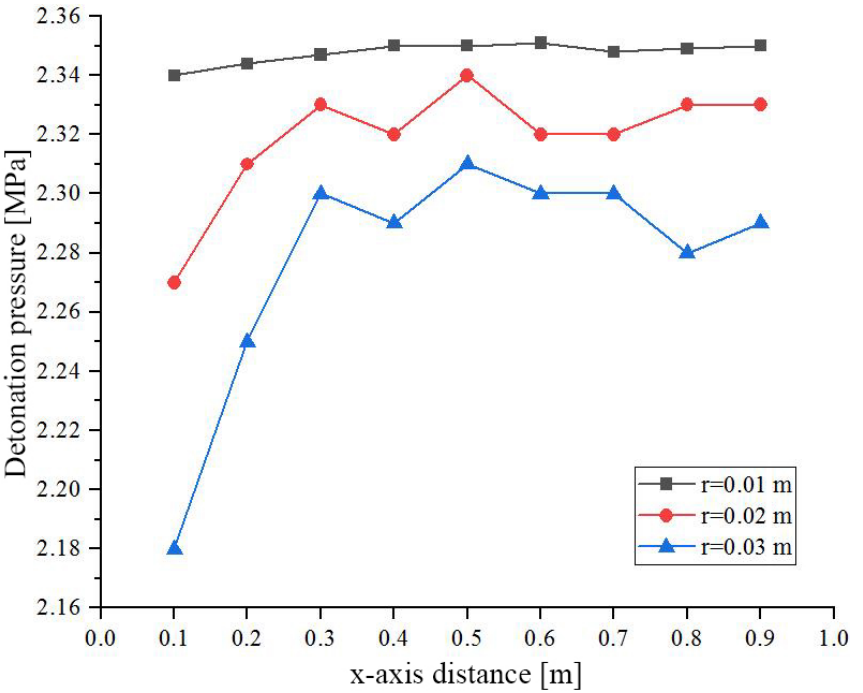


**Figure 7.** Detonation pressure at different radius distance

Figure 7 shows the detonation pressure at different radius distances along the tube. Due to the influence of the wall, the detonation pressure near the wall is slightly lower than the pressure in the center of the tube. This phenomenon is more obvious at the beginning of detonation. At 0.1 m x-axis distance, the maximum pressure difference reaches 0.16 MPa. Furthermore, the pressure at $r$ = 0.01 m is more stable.

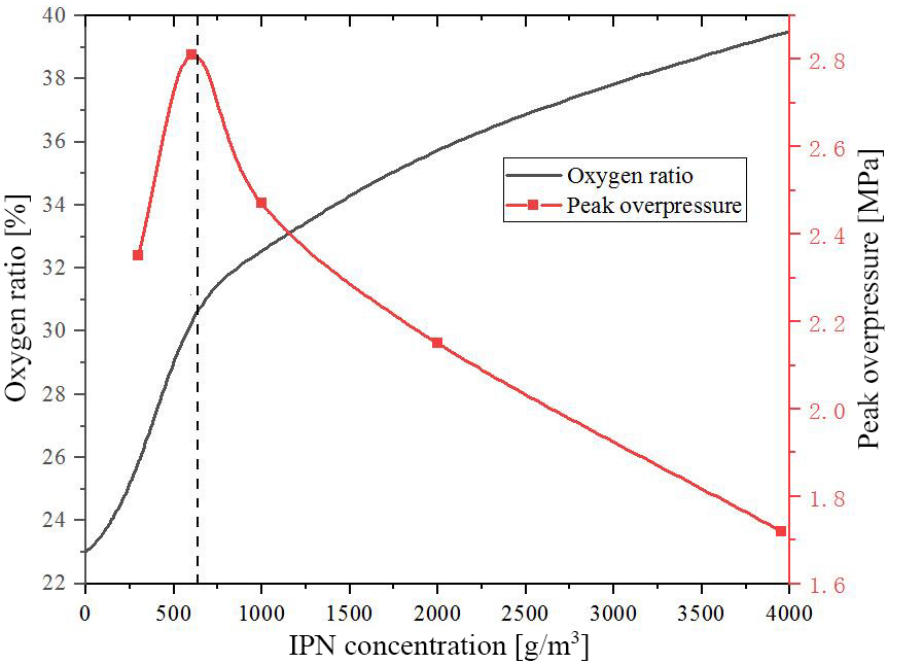


**Figure 8.** Relationship between oxygen ratio and peak overpressure

IPN contains oxygen in its molecular structure. The oxygen ratio from Table 3 can be used to analyze the change in peak overpressure [38]. Figure 8 shows the relationship between the oxygen ratio and the peak overpressure. When the IPN concentration is less than 600 g/m$^3$, the oxygen ratio curve rises rapidly, and the peak overpressure increases accordingly. When the IPN concentration is higher than 600 g/m$^3$, the slope of the oxygen ratio curve decreases, the oxygen ratio increases more slowly at a relatively steady rate, and the peak overpressure begins to decline. It can be predicted that as the IPN concentration continues to increase, the oxygen ratio will begin to decrease and eventually stabilize at 23-24%. This is because when the concentration is too high, the amount of oxygen in the air is negligible, and the oxygen ratio will only represent the amount of oxygen in the molecular structure of the IPN. The lack of oxygen directly inhibits the reaction. The results show that when the oxygen ratio rises rapidly from 23% to 30%, IPN can maintain a high intensity detonation.

## 4.2 Detonation temperature

Figure 9 shows the detonation temperature of different concentrations of IPN/air mixtures. For an oxygen-poor IPN/air mixture, the detonation peak temperature of the 300 g/m$^3$ mixture is the highest, reaching 3440 K. The detonation peak temperature of the 4000 g/m$^3$ mixture is the lowest, at only 2580 K. During this interval, the concentration has increased by 567% and the temperature has decreased by 25%. The peak temperature of the 600 g/m$^3$ mixture is also high, reaching 3370 K. The peak temperature of the 1000 and 2000 g/m$^3$ mixtures decreases successively, the values being 2980 and 2650 K, respectively. The time when the maximum detonation temperature for the 300 g/m$^3$ mixture passes the 0.5 m point is only later than for the 600 g/m$^3$ mixture, and earlier than for any other concentration.

Figure 10 shows a comparison of the detonation peak temperatures at different concentrations. When $\Phi$ = 1-3, the simulated temperature exhibits the same decreasing trend as the experimental temperature [39]. When the fuel concentration is higher than its stoichiometric concentration, the detonation temperature of the IPN/air mixture begins to decrease. The detonation temperature drops rapidly in the range of 600-2000 g/m$^3$. From the perspective of heat release by combustion, the energy released by IPN's complete combustion is 154.81 kJ/mol, and the energy released by IPN's thermal decomposition is 175 kJ/mol [40, 41]. For high concentrations of IPN, the lack of oxygen has a strong inhibiting effect on IPN combustion. The heat released caused by decomposition of the rich fuel is not enough to compensate for the loss of combustion heat caused by the deterioration in the matching relationship between combustible elements and oxygen elements.

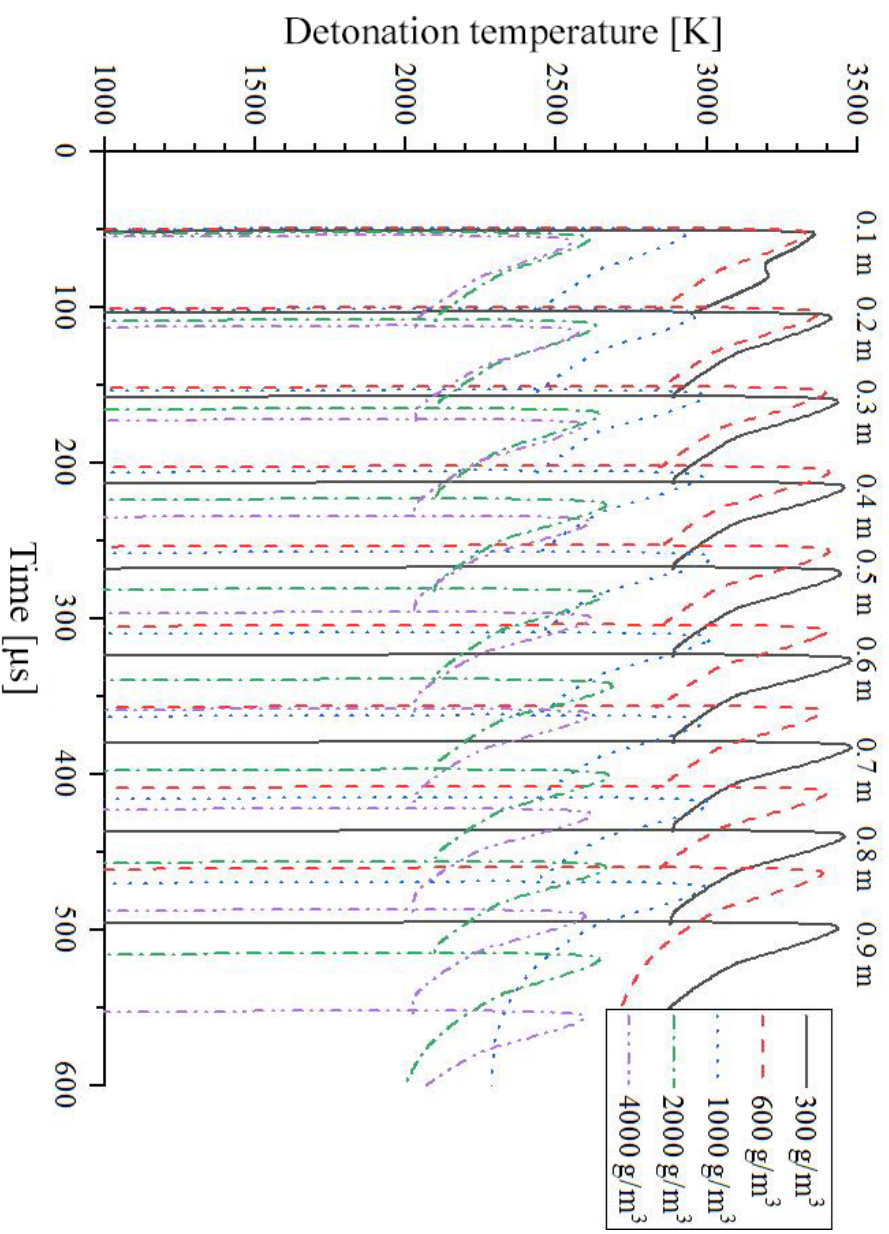


**Figure 9.** Detonation temperatures of IPN/air mixtures at different concentrations

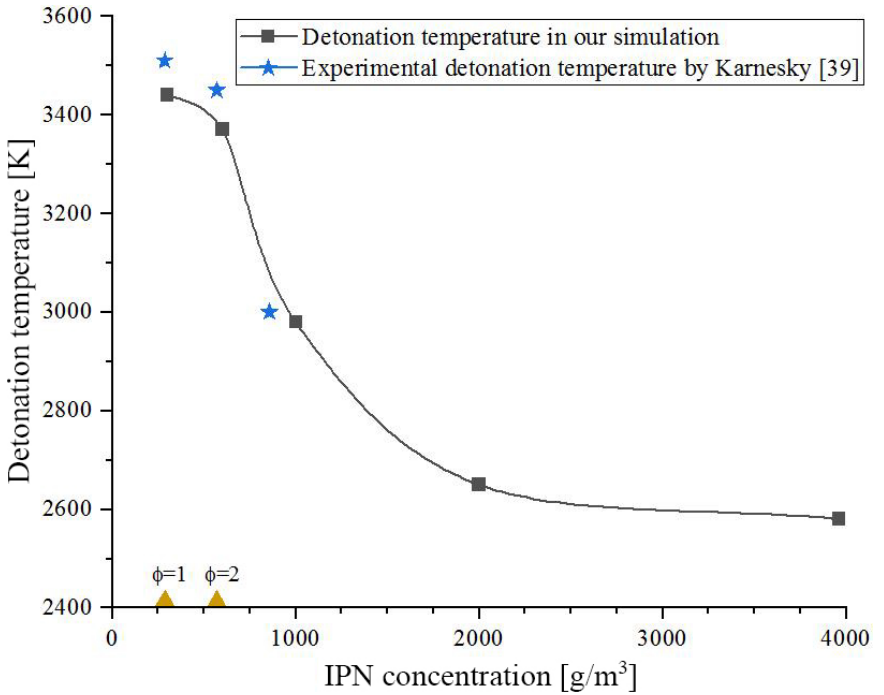


**Figure 10.** Comparison of detonation peak overpressure and peak temperature

## 4.3 Detonation velocity

After the IPN/air premixed gas is ignited at the leftmost end, it gradually develops into a stable detonation in the tube and propagates at a constant speed. The detonation velocity can be calculated according to the time the detonation wave arrives at each monitoring point. Figure 11 shows the detonation velocity of mixtures with different concentrations of the IPN/air mixtures. The detonation velocity here is the average velocity of the nine monitoring points.

The results show that the detonation velocity of the 600 g/m$^3$ IPN mixture is the highest, reaching 1890 m/s. The detonation velocity of the 300 g/m$^3$ mixture is only lower than the 600 g/m$^3$mixture, and higher than any other concentration. The detonation velocity decreases rapidly in the concentration range of 600-4000 g/m$^3$. The detonation velocity of the 4000 g/m$^3$ mixture is the lowest, only 1525 m/s. This trend is consistent with the changes in detonation overpressure. In the concentration range of 300-600 g/m$^3$, fuel density plays a dominant role. The increased concentration means more fuel to react, releasing more energy to support the detonation wave. When the concentration is higher than 600 g/m$^3$, the equivalence ratio is extremely large. The energy provided for detonation

wave propagation is reduced, and the detonation velocity drops.

The results can also be compared with the experimental detonation velocity. It can be found that the simulated velocities are in good agreement with the experimental velocities. Both the simulated and experimental velocity [42] reaches the maximum detonation velocity at almost the same concentration of 600 g/m$^3$. Other reported experimental velocities [9, 37] are slightly lower than the simulated velocities. The maximum experimental velocity (1810 m/s) has a 4.42% difference with the simulation results. The simulated velocities also exhibit the same trend as the CJ detonation velocities when $\Phi$ = 0.5-2.5. In the numerical simulations, fuel loss can be ignored [43]. At the same time, the detonation velocity at the center of the tube is slightly higher than that at the edge. Therefore, the simulated detonation velocity is slightly higher than the experimental data.

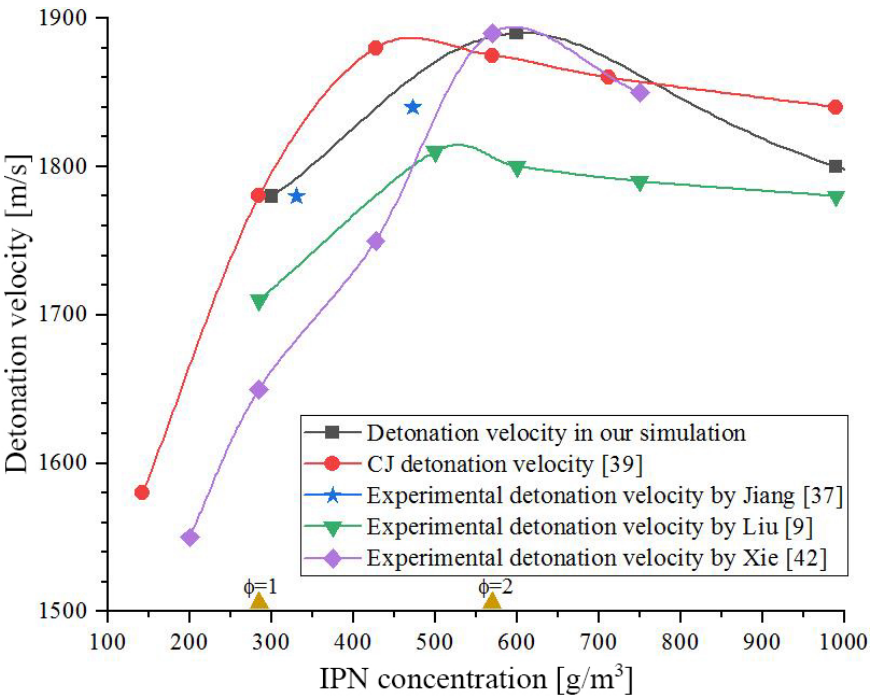


**Figure 11.** Comparison of simulated and experimental detonation velocity

## 4.4 Detonation products

When the detonation wave arrives, the mass fraction of IPN and oxygen will decrease rapidly. With the progress of the chemical reaction, the mass fraction of each reaction product will increase. When oxygen is sufficient, IPN will be fully burned to produce $CO_2$ and $H_2O$. At this time, most of the energy released by IPN combustion is used to support the detonation wave propagation. When oxygen is insufficient, IPN cannot be fully burned, and its main product is $CH_3CHO$. Figure 12 shows the species mass fractions before and after the chemical reaction at the 0.5 m monitoring point. As shown in Figure 12(a), when the IPN concentration is 300 g/m$^3$ ($\Phi = 1.08$), combustion is relatively efficient, and a large amount of $CO_2$ and $H_2O$ are generated, while only a small amount of $CH_3CHO$ is generated. At 600 g/m$^3$, the outputs of $CO_2$, $H_2O$ and $CH_3CHO$ are very large, which indicates the formation of a large number of gaseous products. With a further increase in IPN concentration, the output of $CH_3CHO$ increases, but the output of $CO_2$ and $H_2O$ starts to decrease significantly, and the IPN surplus starts to increase. It is worth noting that when the IPN concentration is below 600 g/m$^3$, almost all of the fuel burns out. At the concentration of 1000 g/m$^3$, the fuel leaves 11% unburnt. At 4000 g/m$^3$, the fuel surplus reaches 32%.

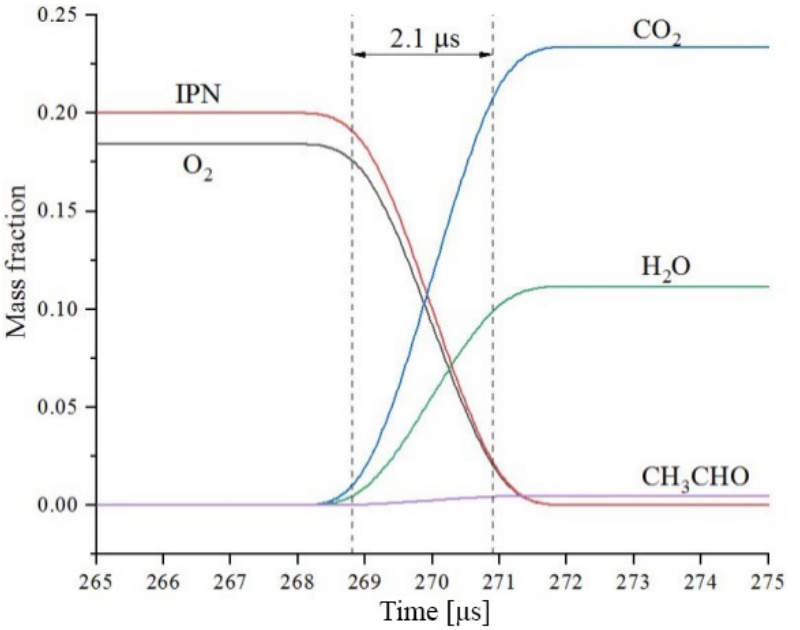


(a)

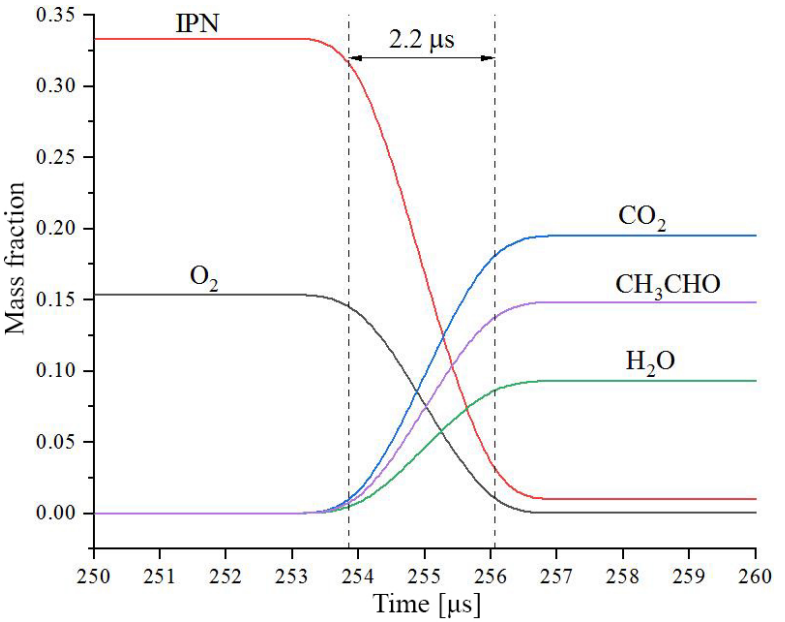


(b)

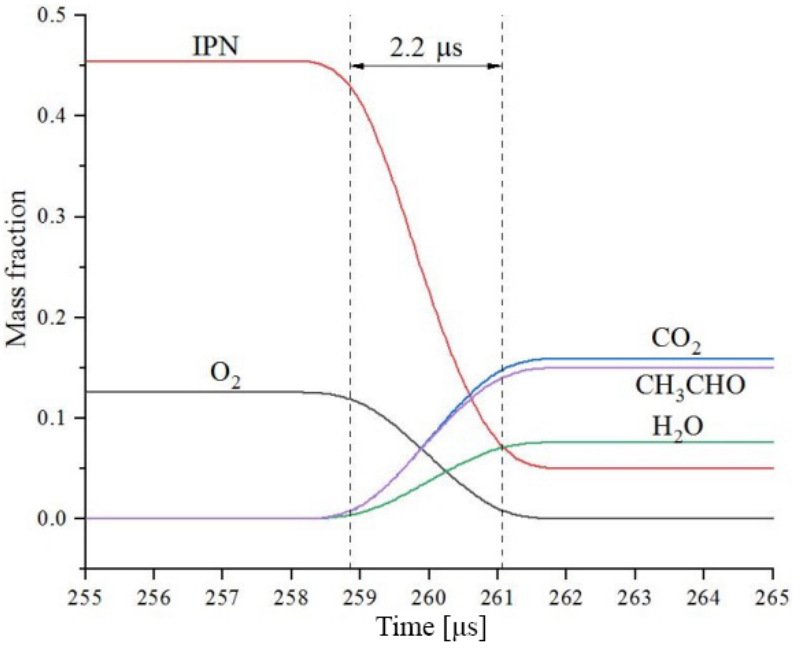


(c)

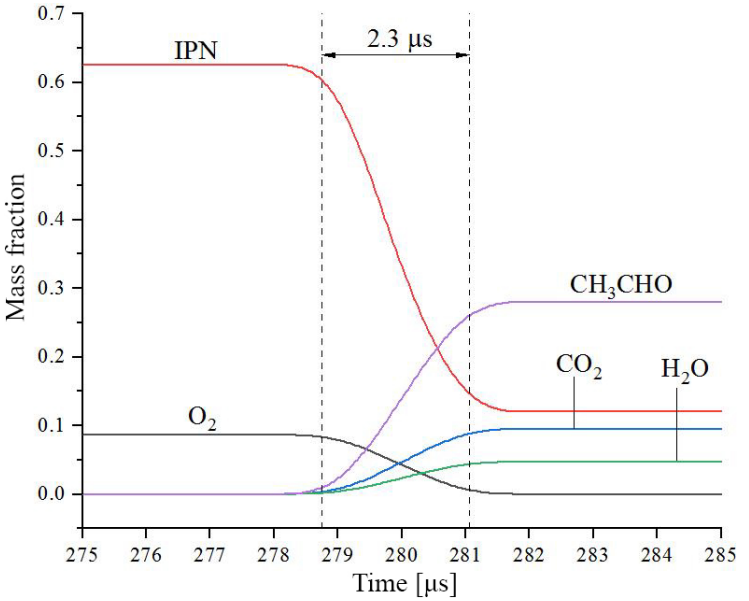


(d)

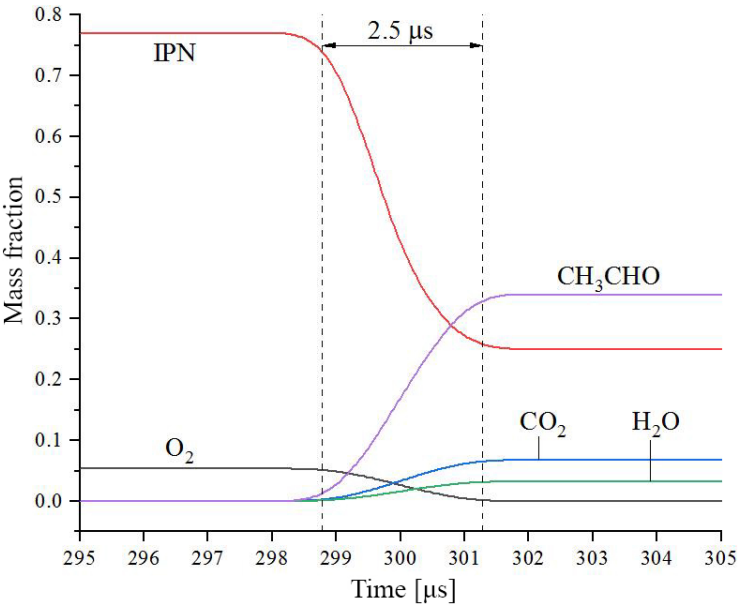


(e)

**Figure 12.** Species mass fraction at the 0.5 m monitoring point for IPN/air at: (a) 300, (b) 600, (c) 1000, (d) 2000, and (e) 4000 g/m$^3$

By comparing the detonation products at different IPN concentrations, it is obvious that the fuel density plays a dominant role when the concentration is 300-600 g/m$^3$. With the increase of IPN concentration, the mass of gaseous products also increases. When the concentration increases by 100%, $CO_2$ and $H_2O$ decrease slightly, but the output of $CH_3CHO$ increases by 1400%. When the IPN concentration is higher than 600 g/m$^3$, the matching relationship between combustible elements and oxygen elements deteriorates seriously, and the oxygen-poor state dominates. When the concentration increases from 600 to 4000 g/m$^3$, $CH_3CHO$ increases by less than 100%, but $CO_2$ and $H_2O$ decrease by more than 200%.

## 5 Conclusions

- Through preliminary simulation of the highly sensitive fuel IPN, it was determined that a stable detonation can be achieved in the detonation tube. The detonation characteristics of high concentrations of gaseous IPN were studied by a two-dimensional numerical simulation.
- The peak values of the IPN detonation characteristics do not occur at the stoichiometric concentration, but at a higher concentration. When $\Phi = 2.15$, the maximum peak overpressure was 2.81 MPa. The peak overpressure of 4000 g/m$^3$ ($\Phi = 14.35$) was 1.72 MPa, which is 61% of the maximum. The peak overpressures of 300 and 2000 g/m$^3$ were close, but these concentrations differs by 566%. Therefore, in the use of IPN fuel, by making the concentration between 300 and 600 g/m$^3$ both excellent detonation properties and low economic cost can be achieved.
- The detonation temperature decreased with the increase in IPN concentration. The detonation temperature was 3440 K at 300 g/m$^3$, and was reduced to 2580 K at 4000 g/m$^3$. Detonation velocity and detonation pressure exhibit similar behaviour. The maximum detonation velocity 1890 m/s was achieved at 600 g/m$^3$ and decreased to 1525 m/s at 4000 g/m$^3$.
- In the fuel-rich state, the incomplete reaction product of IPN is mainly $CH_3CHO$. The formation of a large number of gaseous products results in a sudden increase in pressure. When the concentration was increased from 300 to 600 g/m$^3$, $CO_2$ and $H_2O$ decreased slightly, but the output of $CH_3CHO$ increased by 1400%. Moreover, when the fuel concentration was above 600 g/m$^3$, more than 11% of fuel surplus is produced. At 4000 g/m$^3$, the fuel surplus can reach 32%. Therefore, making the concentration between 300 and 600 g/m$^3$ can achieve both excellent detonation properties and no fuel waste.

## Acknowledgements

The research presented in this paper was supported by the National Natural Science Foundation of China (11772057, 11972089).

## References

[1] Ambekar, A.; Chowdhury, A.; Challa, S.; Radhakrishna, D. Droplet Combustion Studies of Hydrocarbon-monopropellant Blends. *Fuel* **2014**, *115*: 697-705.
[2] Zhou, J.; Ding, L.; An, J.; Zhu, Y.; Liang, Y. Study on the Thermal Behaviors of Nano-Al Based Fuel Air Explosive. *J. Therm. Anal. Calorim.* **2017**, *130*: 1111-1116.
[3] Zhang, F.; Murray, S.; Yoshinaka, A.; Higgins, A. Shock Initiation and Detonability of Isopropyl Nitrate. *12th Int. Detonation Symp.,* San Diego, CA, **2002**, 781-790.
[4] Mbugua, A.; Satija, A.; Lucht, R.; Bane, S. Ignition and Combustion Characterization of Single Nitromethane and Isopropyl Nitrate Monopropellant Droplets under High-temperature and quasi-Steady Conditions. *Combust. Flame* **2020**, *212*: 295-308.
[5] Roy, G.D.; Frolov, S.M.; Borisov, A.A.; Netzer, D.W. Pulse Detonation Propulsion: Challenges, Current Status, and Future Perspective. *Prog. Energ. Combust.* **2004**, *30*: 545-672.
[6] Gifford, M.J.; Proud, W.G.; Field, J.E. Development of a Method for Quantification of Hot-Spots. *Thermochim. Acta* **2002**, *384*: 285-290.
[7] Hedlund, F.H.; Nielsen, M.F.; Mikkelsen, S.H.; Kragh, E.K. Violent Explosion after Inadvertent Mixing of Nitric Acid and Isopropanol – Review 15 Years Later Finds Basic Accident Data Corrupted, no Evidence of Broad Learning. *Safety Sci*. **2014**, *70*: 255-261.
[8] Ambekar, A.; Sreedhara, S.; Chowdhury, A. Burn Rate Characterization of iso-Propyl Nitrate – A Neglected Monopropellant. *Combust. Flame* **2015**, *162*: 836-845.
[9] Liu, Q.; Bai, C.; Dai, W.; Jiang, L. Deflagration-to-Detonation Transition in Isopropyl Nitrate Mist/Air Mixtures. *Combust. Explo. Shock+* **2011**, *47*(4): 488-456.
[10] Sheffield, S.; Davis, L.; Baer, M.; Engelke, R.; Alcon, R.R.; Renlund, A.M. Hugoniot and Shock Initiation Studies of Isopropyl Nitrate. *AIP Conf. Proc.* **2002**, *620*: 1051-1054.
[11] Nassim, B.; Zhang, Q. Thermal Stability of Explosive Mixture with Additives at Different Ambient Temperatures. *Propellants Explos., Pyrotech*. **2018**, *43*: 177-187.
[12] Liu, X.; Wang, Y. A Comparative Study of the Explosion Characteristics of IPN and IPN/JP-10 Mixtures in Air Aerosols. *Propellants Explos., Pyrotech*. **2017**, *42*: 1222-1232.
[13] Wang, H.; Sun, X.; Rao, G.; Jian, G.; Xie, L. The Critical Energy of Direct Initiation in Liquid Fuel-Air and Liquid Fuel-RDX Powder-Air Mixtures in a Vertical Detonation Tube. *Propellants Explos., Pyrotech*. **2014**, *39*: 597-603.
[14] Yao, G.; Zhang, B.; Xiu, G.; Bai, C.; Liu, P. The Critical Energy of Direct Initiation and Detonation Cell Size in Liquid Hydrocarbon Fuel/Air Mixtures. *Fuel* **2013**,

*113*: 331-339.
[15] Zhang, Q.; Qian, X.; Fu, L.; Yuan, M.; Chen, Y. Shock Wave Evolution and Overpressure Hazards in Partly Premixed Gas Deflagration of DME/LPG Blended Multi-Clean Fuel. *Fuel* **2020**, *268*: 117368.
[16] Liu, L.; Zhang, Q. Comparison of Detonation Characteristics for Typical Binary Blended Fuel. *Fuel* **2020**, *268*: 117351.
[17] Song, Y.; Zhang, Q. Explosion Effect of Vapor-Liquid Two-Phase n-Heptane at Various Initial Temperatures. *Process Saf. Environ. Prot.* **2021**, *145*: 303-311.
[18] Batchelor, G.K. *An Introduction to Fluid Dynamics.* Cambridge Univ. Press, England, **1967**, pp. 138-139; ISBN 978-0-521-66396-2.
[19] Magnussen, B.F.; Hjertager, B.H. On Mathematical Modeling of Turbulent Combustion with Special Emphasis on Soot Formation and Combustion. *Symp. (Int'l) on Combustion,* **1977**, *16*: 719-729.
[20] Launder, B.E.; Spalding, D.B. *Lectures in Mathematical Models of Turbulence.* Academic Press, London, **1972**.
[21] Modest, M. *Radiative Heat Transfer. 2nd ed.*, Academic Press, New York, **2003**; ISBN 9780125031639.
[22] Wakeman, T.; Tabakoff, W. *Measured Particle Rebound Characteristics Useful for Erosion Prediction.* ASME paper 82-GT-170, **1982**.
[23] Morin, J.; Bedjanian, Y. Thermal Decomposition of Isopropyl Nitrate: Kinetics and Products. *J. Phys. Chem. A* **2016**, *120*(41): 8037-8043.
[24] Chen, Y.; An, Z.; Chen, M.; Zhang, L. Quantum Chemistry Calculation of Hydrolysis Reaction of Isopropyl Nitrate. (in Chinese) *Chin. J. Explos. Propellants (Huozhayao Xuebao)* **2018**, *41*(5): 517-522.
[25] Swami, U.; Ambekar, A.; Gondge, D.; Sreedhara, S.; Chowdhury, A. Burn Rate Characterization of Desensitized Isopropyl Nitrate Blends. *Combust. Flame* **2018**, *190*: 454-466.
[26] Gong, X.D.; Xiao, H.M. Studies on the Molecular Structures, Vibrational Spectra and Thermodynamic Properties of Organic Nitrates using Density Functional Theory and *ab initio* Methods. *J. Mol. Struc-Theochem*. **2001**, *572*: 213-221.
[27] Ghahremanpour, M; van Maaren, P.J.; Ditz, J.C.; Lindh, R.; van der Spoel, D. Large-scale Calculations of Gas Phase Thermochemistry: Enthalpy of Formation, Standard Entropy, and Heat Capacity. *J. Chem. Phys*. **2016**, *145*, paper 114305: 1-12.
[28] Liu, X.; Ma, Y.; Li, S.; Yan, H.; Wang, D.; Luo, Y. Study of the Reaction Mechanism of Aluminum Based Composite Fuel and Chlorine Trifluoride Oxide. *Energy* **2019**, *168*: 393-399.
[29] Beeley, P.; Griffiths, J.F.; Gray, P. Rapid Compression Studies on Spontaneous Ignition of Isopropyl Nitrate Part II: Rapid Sampling, Intermediate Stages and Reaction Mechanisms. *Combust. Flame* **1980**, *39*(3): 269-281.
[30] Zeng, X.; Chen, W.; Liu, J.; Kan, J. Study on NPN and IPN using Density Functional Theory. (in Chinese) *Comput. Appl. Chem.* **2008**, *25*(2): 201-204.
[31] Oxley, J.; Smith, J.; Rogers, E.; Ye, W. Heat-Release Behavior of Fuel Combustion

Additives. *Energ. Fuel* **2001**, *15*: 1194-1199.
[32] Zeng, X.; Chen, W.; Liu, J. Molecular Structure, Electronic Structure and Heats of Formation of Explosive Sensitizers. (in Chinese) *Acta Phys.-Chim. Sin*. **2007**, *23*(2): 192-197.
[33] Krause, H.; Eisenreich, N.; Pfeil, A. Kinetics of Evaporation and Decomposition of Isopropyl Nitrate by Rapid Scan IR Spectroscopy. *Thermochim. Acta* **1989**, *149*: 349-356.
[34] Jones, D.E.G.; Feng, H.T.; Augsten, R.A.; Fouchard, R.C. Thermal Analysis Studies on Isopropyl Nitrate. *J. Therm. Anal. Calorim*. **1999**, *55*: 9-19.
[35] Xing, X.; Zhao, S.; Li, W.; Fang, W. The Reactivity between Aluminum Powder and Liquid Phase of Fuel-Air Explosives. (in Chinese) *Chin. J. Explos. Propellants (Huozhayao Xuebao)* **2016**, *39*(6): 55-57.
[36] Liu, L.; Zhang, Q. Comparison of Detonation Characteristics in Energy Output of Gaseous JP-10 and Propylene Oxide in Air. *Fuel* **2018**, *232*: 154-164.
[37] Jiang, L.; Bai, C.; Liu, Q. Experimental Study on DDT Process in 3-Phase Suspensions of Gas/Solid Particle/Liquid Mist Mixture. (in Chinese) *Explos. Shock Waves* **2010**, *30*(6): 588-592.
[38] Zhong, Y.; Wu, Y.; Jin, D.; Chen, X.; Yang, X.; Wang, S. Investigation of Rotating Detonation Fueled by the Pre-Combustion Cracked Kerosene. *Aerosp. Sci. Technol*. **2019**, *95*, paper 105480: 1-8.
[39] Karnesky, J.; Pitz, W.J.; Shepherd, J.E. Detonation in Gaseous Isopropyl Nitrate Mixtures. *2007 Fall Meeting of the Western States Section of the Combustion Institute Sandia National Laboratories*, Livermore, CA, **2007**, 07F-40.
[40] Borisov, A.A.; Troshin, K.Ya.; Mikhalkin, V.N. Ignition and Combustion of Isopropyl Nitrate. *Russ. J. Phys. Chem. B* **2016**, *10*(5): 780-784.
[41] Griffiths, J.F.; Gilligan, M.F.; Gray, P. Pyrolysis of Isopropyl Nitrate. I. Decomposition at Low Temperatures and Pressures. *Combust. Flame* **1975**, *24*: 11-19.
[42] Xie, L.; Li, B.; Zhang, Y. Experimental Study on Detonation Parameters and Cellular Structures of Fuel Cloud. *Acta Mech. Sin*. **2012**, *28*(2): 438-443.
[43] Adebiyi, A.; Alkandari, R.; Valiev, D.; Akkerman, V. Effect of Surface Friction on Ultrafast Flame Acceleration in Obstructed Cylindrical Pipes. *AIP Adv*. **2019**, *9*(3) paper 035249: 1-6.

Received: February 15, 2021
Revised: June 25, 2021
First published online: June 30, 2021